Measurement of the transverse spin correlation in $Z \to \tau^+\tau^-$ decays

P. Abreu, W. Adam, T. Adye, I. Ajinenko, G D. Alekseev, R. Alemany, P P. Allport, S. Almehed, S. Amato, P. Andersson, et al.

EUROPEAN ORGANIZATION FOR NUCLEAR RESEARCH

CERN–PPE/97–34

27 March 1997

Measurement of the transverse spin correlation in $Z \to \tau^+\tau^-$ decays

DELPHI Collaboration

Abstract

The measurement of the correlation between the transverse spin components of $\tau^+\tau^-$ pairs collected during 1992 to 1994 with the DELPHI detector at LEP1 is presented. A value

$$C_{TT} = 0.87 \pm 0.20 \text{ (stat.)} \, ^{+\ 0.10}_{-\ 0.12} \text{ (syst.)}$$

was obtained for the correlation parameter, in agreement with the Standard Model expectation.

(To be submitted to Physics Letters B)

P.Abreu[21], W.Adam[49], T.Adye[36], I.Ajinenko[41], G.D.Alekseev[16], R.Alemany[48], P.P.Allport[22], S.Almehed[24], U.Amaldi[9], S.Amato[46], P.Andersson[43], A.Andreazza[9], P.Antilogus[9], W-D.Apel[17], B.Åsman[43], J-E.Augustin[25], A.Augustinus[30], P.Baillon[9], P.Bambade[19], F.Barao[21], M.Barbi[46], D.Y.Bardin[16], G.Barker[9], A.Baroncelli[39], O.Barring[24], M.J.Bates[36], M.Battaglia[15], M.Baubillier[23], J.Baudot[38], K-H.Becks[51], M.Begalli[6], P.Beilliere[8], Yu.Belokopytov[9,52], K.Belous[41], A.C.Benvenuti[5], M.Berggren[46], D.Bertini[25], D.Bertrand[2], M.Besancon[38], F.Bianchi[44], M.Bigi[44], M.S.Bilenky[16], P.Billoir[23], M-A.Bizouard[19], D.Bloch[10], M.Blume[51], M.Bonesini[27], W.Bonivento[27], P.S.L.Booth[22], A.W.Borgland[4], G.Borisov[38,41], C.Bosio[39], O.Botner[47], E.Boudinov[30], B.Bouquet[19], C.Bourdarios[19], T.J.V.Bowcock[22], I.Bozovic[11], M.Bozzo[13], P.Branchini[39], K.D.Brand[35], T.Brenke[51], R.A.Brenner[47], C.Bricman[2], R.C.A.Brown[9], P.Bruckman[18], J-M.Brunet[8], L.Bugge[32], T.Buran[32], T.Burgsmueller[51], P.Buschmann[51], S.Cabrera[48], M.Caccia[27], M.Calvi[27], A.J.Camacho Rozas[40], T.Camporesi[9], V.Canale[37], M.Canepa[13], F.Cao[2], F.Carena[9], L.Carroll[22], C.Caso[13], M.V.Castillo Gimenez[48], A.Cattai[9], F.R.Cavallo[5], V.Chabaud[9], Ph.Charpentier[9], L.Chaussard[25], P.Checchia[35], G.A.Chelkov[16], M.Chen[2], R.Chierici[44], P.Chliapnikov[41], P.Chochula[7], V.Chorowicz[25], V.Cindro[42], P.Collins[9], R.Contri[13], E.Cortina[48], G.Cosme[19], F.Cossutti[45], J-H.Cowell[22], H.B.Crawley[1], D.Crennell[36], G.Crosetti[13], J.Cuevas Maestro[33], S.Czellar[15], J.Dahm[51], B.Dalmagne[19], M.Dam[28], G.Damgaard[28], P.D.Dauncey[36], M.Davenport[9], W.Da Silva[23], A.Deghorain[2], G.Della Ricca[45], P.Delpierre[26], N.Demaria[34], A.De Angelis[9], W.De Boer[17], S.De Brabandere[2], C.De Clercq[2], C.De La Vaissiere[23], B.De Lotto[45], A.De Min[35], L.De Paula[46], H.Dijkstra[9], L.Di Ciaccio[37], A.Di Diodato[37], A.Djannati[8], J.Dolbeau[8], K.Doroba[50], M.Dracos[10], J.Drees[51], K.-A.Drees[51], M.Dris[31], J-D.Durand[25,9], D.Edsall[1], R.Ehret[17], G.Eigen[4], T.Ekelof[47], G.Ekspong[43], M.Elsing[9], J-P.Engel[10], B.Erzen[42], M.Espirito Santo[21], E.Falk[24], G.Fanourakis[11], D.Fassouliotis[45], M.Feindt[9], P.Ferrari[27], A.Ferrer[48], S.Fichet[23], T.A.Filippas[31], A.Firestone[1], P.-A.Fischer[10], H.Foeth[9], E.Fokitis[31], F.Fontanelli[13], F.Formenti[9], B.Franek[36], A.G.Frodesen[4], R.Fruhwirth[49], F.Fulda-Quenzer[19], J.Fuster[48], A.Galloni[22], D.Gamba[44], M.Gandelman[46], C.Garcia[48], J.Garcia[40], C.Gaspar[9], U.Gasparini[35], Ph.Gavillet[9], E.N.Gazis[31], D.Gele[10], J-P.Gerber[10], R.Gokieli[50], B.Golob[42], P.Goncalves[21], G.Gopal[36], L.Gorn[1], M.Gorski[50], Yu.Gouz[44,52], V.Gracco[13], E.Graziani[39], C.Green[22], A.Grefrath[51], P.Gris[38], G.Grosdidier[19], K.Grzelak[50], S.Gumenyuk[41], M.Gunther[47], J.Guy[36], F.Hahn[9], S.Hahn[51], Z.Hajduk[18], A.Hallgren[47], K.Hamacher[51], F.J.Harris[34], V.Hedberg[24], R.Henriques[21], J.J.Hernandez[48], P.Herquet[2], H.Herr[9], T.L.Hessing[34], J.-M.Heuser[51], E.Higon[48], H.J.Hilke[9], S-O.Holmgren[43], P.J.Holt[34], D.Holthuizen[30], S.Hoorelbeke[2], M.Houlden[22], J.Hrubec[49], K.Huet[2], K.Hultqvist[43], J.N.Jackson[22], R.Jacobsson[43], P.Jalocha[9], R.Janik[7], Ch.Jarlskog[24], G.Jarlskog[24], P.Jarry[38], B.Jean-Marie[19], E.K.Johansson[43], L.Jonsson[24], P.Jonsson[24], C.Joram[9], P.Juillot[10], M.Kaiser[17], F.Kapusta[23], K.Karafasoulis[11], M.Karlsson[43], S.Katsanevas[25], E.C.Katsoufis[31], R.Keranen[4], Yu.Khokhlov[41], B.A.Khomenko[16], N.N.Khovanski[16], B.King[22], N.J.Kjaer[30], O.Klapp[51], H.Klein[9], P.Kluit[30], D.Knoblauch[17], B.Koene[30], P.Kokkinias[11], A.Konopliannikov[41], M.Koratzinos[9], K.Korcyl[18], V.Kostioukhine[41], C.Kourkoumelis[3], O.Kouznetsov[13,16], M.Krammer[49], C.Kreuter[9], I.Kronkvist[24], Z.Krumstein[16], W.Krupinski[18], P.Kubinec[7], W.Kucewicz[18], K.Kurvinen[15], C.Lacasta[9], I.Laktineh[25], J.W.Lamsa[1], L.Lanceri[45], D.W.Lane[1], P.Langefeld[51], J-P.Laugier[38], R.Lauhakangas[15], G.Leder[49], F.Ledroit[14], V.Lefebure[2], C.K.Legan[1], A.Leisos[11], R.Leitner[29], J.Lemonne[2], G.Lenzen[51], V.Lepeltier[19], T.Lesiak[18], J.Libby[34], D.Liko[9], R.Lindner[51], A.Lipniacka[43], I.Lippi[35], B.Loerstad[24], J.G.Loken[34], J.M.Lopez[40], D.Loukas[11], P.Lutz[38], L.Lyons[34], J.MacNaughton[49], G.Maehlum[17], J.R.Mahon[6], A.Maio[21], T.G.M.Malmgren[43], V.Malychev[16], F.Mandl[49], J.Marco[40], R.Marco[40], B.Marechal[46], M.Margoni[35], J-C.Marin[9], C.Mariotti[9], A.Markou[11], C.Martinez-Rivero[33], F.Martinez-Vidal[48], S.Marti i Garcia[22], F.Matorras[40], C.Matteuzzi[27], G.Matthiae[37], M.Mazzucato[35], M.Mc Cubbin[22], R.Mc Kay[1], R.Mc Nulty[9], J.Medbo[47], M.Merk[30], C.Meroni[27], S.Meyer[17], W.T.Meyer[1], A.Miagkov[41], M.Michelotto[35], E.Migliore[44], L.Mirabito[25], W.A.Mitaroff[49], U.Mjoernmark[24], T.Moa[43], R.Moeller[28], K.Moenig[9], M.R.Monge[13], P.Morettini[13], H.Mueller[17], K.Muenich[51], M.Mulders[30], L.M.Mundim[6], W.J.Murray[36], B.Muryn[14,18], G.Myatt[34], F.Naraghi[14], F.L.Navarria[5], S.Navas[48], K.Nawrocki[50], P.Negri[27], S.Nemecek[12], W.Neumann[51], N.Neumeister[49], R.Nicolaidou[3], B.S.Nielsen[28], M.Nieuwenhuizen[30], V.Nikolaenko[10], M.Nikolenko[10,16], P.Niss[43], A.Nomerotski[35], A.Normand[34], M.Novak[12], W.Oberschulte-Beckmann[17], V.Obraztsov[41], A.G.Olshevski[16], A.Onofre[21], R.Orava[15], G.Orazi[10], K.Osterberg[15], A.Ouraou[38], P.Paganini[19], M.Paganoni[9,27], P.Pages[10], R.Pain[23], H.Palka[18], Th.D.Papadopoulou[31], K.Papageorgiou[11], L.Pape[9], C.Parkes[34], F.Parodi[13], A.Passeri[39], M.Pegoraro[35], L.Peralta[21], H.Pernegger[49], M.Pernicka[49], A.Perrotta[5], C.Petridou[45], A.Petrolini[13], H.T.Phillips[36], G.Piana[13], F.Pierre[38], M.Pimenta[21], T.Podobnik[42], O.Podobrin[9], M.E.Pol[6], G.Polok[18], P.Poropat[45], V.Pozdniakov[16], P.Privitera[37], N.Pukhaeva[16], A.Pullia[27], D.Radojicic[34], S.Ragazzi[27], H.Rahmani[31], J.Rames[12], P.N.Ratoff[20], A.L.Read[32], M.Reale[51], P.Rebecchi[19], N.G.Redaelli[27], D.Reid[9], R.Reinhardt[51], P.B.Renton[34], L.K.Resvanis[3], F.Richard[19], J.Richardson[22], J.Ridky[12], G.Rinaudo[44], A.Romero[44], I.Roncagliolo[13], P.Ronchese[35], L.Roos[23], E.I.Rosenberg[1], P.Roudeau[19], T.Rovelli[5], W.Ruckstuhl[30], V.Ruhlmann-Kleider[38], A.Ruiz[40], K.Rybicki[18], H.Saarikko[15], Y.Sacquin[38], A.Sadovsky[16], O.Sahr[14], G.Sajot[14], J.Salt[48], M.Sannino[13], H.Schneider[17], U.Schwickerath[17], M.A.E.Schyns[51], G.Sciolla[44], F.Scuri[45], P.Seager[20], Y.Sedykh[16], A.M.Segar[34], A.Seitz[17], R.Sekulin[36], L.Serbelloni[37], R.C.Shellard[6], P.Siegrist[9,38], R.Silvestre[38], F.Simonetto[35], A.N.Sisakian[16], B.Sitar[7], T.B.Skaali[32], G.Smadja[25], N.Smirnov[41], O.Smirnova[24], G.R.Smith[36], A.Sokolov[41], O.Solovianov[41], R.Sosnowski[50], D.Souza-Santos[6], T.Spassov[21], E.Spiriti[39], P.Sponholz[51], S.Squarcia[13], D.Stampfer[9], C.Stanescu[39], S.Stanic[42], S.Stapnes[32], I.Stavitski[35], K.Stevenson[34], A.Stocchi[19], J.Strauss[49], R.Strub[10], B.Stugu[4], M.Szczekowski[50], M.Szeptycka[50], T.Tabarelli[27], J.P.Tavernet[23], O.Tchikilev[41], F.Tegenfeldt[47], F.Terranova[27], J.Thomas[34], A.Tilquin[26], J.Timmermans[30],

L.G.Tkatchev[16], T.Todorov[10], S.Todorova[10], D.Z.Toet[30], A.Tomaradze[2], B.Tome[21], A.Tonazzo[27], L.Tortora[39], G.Transtromer[24], D.Treille[9], G.Tristram[8], A.Trombini[19], C.Troncon[27], A.Tsirou[9], M-L.Turluer[38], I.A.Tyapkin[16], M.Tyndel[36], S.Tzamarias[11], B.Ueberschaer[51], O.Ullaland[9], V.Uvarov[41], G.Valenti[5], E.Vallazza[45], C.Vander Velde[2], G.W.Van Apeldoorn[30], P.Van Dam[30], W.K.Van Doninck[2], J.Van Eldik[30], A.Van Lysebetten[2], N.Vassilopoulos[34], G.Vegni[27], L.Ventura[35], W.Venus[36], F.Verbeure[2], M.Verlato[35], L.S.Vertogradov[16], D.Vilanova[38], P.Vincent[25], L.Vitale[45], A.S.Vodopyanov[16], V.Vrba[12], H.Wahlen[51], C.Walck[43], F.Waldner[45], P.Weilhammer[9], C.Weiser[17], A.M.Wetherell[9], D.Wicke[51], J.H.Wickens[2], M.Wielers[17], G.R.Wilkinson[9], W.S.C.Williams[34], M.Winter[10], M.Witek[18], T.Wlodek[19], J.Yi[1], K.Yip[34], O.Yushchenko[41], F.Zach[25], A.Zaitsev[41], A.Zalewska[9], P.Zalewski[50], D.Zavrtanik[42], E.Zevgolatakos[11], N.I.Zimin[16], D.Zontar[42], G.C.Zucchelli[43], G.Zumerle[35]

[1] Department of Physics and Astronomy, Iowa State University, Ames IA 50011-3160, USA
[2] Physics Department, Univ. Instelling Antwerpen, Universiteitsplein 1, B-2610 Wilrijk, Belgium
and IIHE, ULB-VUB, Pleinlaan 2, B-1050 Brussels, Belgium
and Faculté des Sciences, Univ. de l'Etat Mons, Av. Maistriau 19, B-7000 Mons, Belgium
[3] Physics Laboratory, University of Athens, Solonos Str. 104, GR-10680 Athens, Greece
[4] Department of Physics, University of Bergen, Allégaten 55, N-5007 Bergen, Norway
[5] Dipartimento di Fisica, Università di Bologna and INFN, Via Irnerio 46, I-40126 Bologna, Italy
[6] Centro Brasileiro de Pesquisas Físicas, rua Xavier Sigaud 150, RJ-22290 Rio de Janeiro, Brazil
and Depto. de Física, Pont. Univ. Católica, C.P. 38071 RJ-22453 Rio de Janeiro, Brazil
and Inst. de Física, Univ. Estadual do Rio de Janeiro, rua São Francisco Xavier 524, Rio de Janeiro, Brazil
[7] Comenius University, Faculty of Mathematics and Physics, Mlynska Dolina, SK-84215 Bratislava, Slovakia
[8] Collège de France, Lab. de Physique Corpusculaire, IN2P3-CNRS, F-75231 Paris Cedex 05, France
[9] CERN, CH-1211 Geneva 23, Switzerland
[10] Centre de Recherche Nucléaire, IN2P3 - CNRS/ULP - BP20, F-67037 Strasbourg Cedex, France
[11] Institute of Nuclear Physics, N.C.S.R. Demokritos, P.O. Box 60228, GR-15310 Athens, Greece
[12] FZU, Inst. of Physics of the C.A.S. High Energy Physics Division, Na Slovance 2, 180 40, Praha 8, Czech Republic
[13] Dipartimento di Fisica, Università di Genova and INFN, Via Dodecaneso 33, I-16146 Genova, Italy
[14] Institut des Sciences Nucléaires, IN2P3-CNRS, Université de Grenoble 1, F-38026 Grenoble Cedex, France
[15] Helsinki Institute of Physics, HIP, P.O. Box 9, FIN-00014 Helsinki, Finland
[16] Joint Institute for Nuclear Research, Dubna, Head Post Office, P.O. Box 79, 101 000 Moscow, Russian Federation
[17] Institut für Experimentelle Kernphysik, Universität Karlsruhe, Postfach 6980, D-76128 Karlsruhe, Germany
[18] Institute of Nuclear Physics and University of Mining and Metalurgy, Ul. Kawiory 26a, PL-30055 Krakow, Poland
[19] Université de Paris-Sud, Lab. de l'Accélérateur Linéaire, IN2P3-CNRS, Bât. 200, F-91405 Orsay Cedex, France
[20] School of Physics and Chemistry, University of Lancaster, Lancaster LA1 4YB, UK
[21] LIP, IST, FCUL - Av. Elias Garcia, 14-1°, P-1000 Lisboa Codex, Portugal
[22] Department of Physics, University of Liverpool, P.O. Box 147, Liverpool L69 3BX, UK
[23] LPNHE, IN2P3-CNRS, Universités Paris VI et VII, Tour 33 (RdC), 4 place Jussieu, F-75252 Paris Cedex 05, France
[24] Department of Physics, University of Lund, Sölvegatan 14, S-22363 Lund, Sweden
[25] Université Claude Bernard de Lyon, IPNL, IN2P3-CNRS, F-69622 Villeurbanne Cedex, France
[26] Univ. d'Aix - Marseille II - CPP, IN2P3-CNRS, F-13288 Marseille Cedex 09, France
[27] Dipartimento di Fisica, Università di Milano and INFN, Via Celoria 16, I-20133 Milan, Italy
[28] Niels Bohr Institute, Blegdamsvej 17, DK-2100 Copenhagen 0, Denmark
[29] NC, Nuclear Centre of MFF, Charles University, Areal MFF, V Holesovickach 2, 180 00, Praha 8, Czech Republic
[30] NIKHEF, Postbus 41882, NL-1009 DB Amsterdam, The Netherlands
[31] National Technical University, Physics Department, Zografou Campus, GR-15773 Athens, Greece
[32] Physics Department, University of Oslo, Blindern, N-1000 Oslo 3, Norway
[33] Dpto. Fisica, Univ. Oviedo, Avda. Calvo Sotelo, S/N-33007 Oviedo, Spain, (CICYT-AEN96-1681)
[34] Department of Physics, University of Oxford, Keble Road, Oxford OX1 3RH, UK
[35] Dipartimento di Fisica, Università di Padova and INFN, Via Marzolo 8, I-35131 Padua, Italy
[36] Rutherford Appleton Laboratory, Chilton, Didcot OX11 OQX, UK
[37] Dipartimento di Fisica, Università di Roma II and INFN, Tor Vergata, I-00173 Rome, Italy
[38] CEA, DAPNIA/Service de Physique des Particules, CE-Saclay, F-91191 Gif-sur-Yvette Cedex, France
[39] Istituto Superiore di Sanità, Ist. Naz. di Fisica Nucl. (INFN), Viale Regina Elena 299, I-00161 Rome, Italy
[40] Instituto de Fisica de Cantabria (CSIC-UC), Avda. los Castros, S/N-39006 Santander, Spain, (CICYT-AEN96-1681)
[41] Inst. for High Energy Physics, Serpukov P.O. Box 35, Protvino, (Moscow Region), Russian Federation
[42] J. Stefan Institute, Jamova 39, SI-1000 Ljubljana, Slovenia and Department of Astroparticle Physics, School of Environmental Sciences, Kostanjeviska 16a, Nova Gorica, SI-5000 Slovenia,
and Department of Physics, University of Ljubljana, SI-1000 Ljubljana, Slovenia
[43] Fysikum, Stockholm University, Box 6730, S-113 85 Stockholm, Sweden
[44] Dipartimento di Fisica Sperimentale, Università di Torino and INFN, Via P. Giuria 1, I-10125 Turin, Italy
[45] Dipartimento di Fisica, Università di Trieste and INFN, Via A. Valerio 2, I-34127 Trieste, Italy
and Istituto di Fisica, Università di Udine, I-33100 Udine, Italy
[46] Univ. Federal do Rio de Janeiro, C.P. 68528 Cidade Univ., Ilha do Fundão BR-21945-970 Rio de Janeiro, Brazil
[47] Department of Radiation Sciences, University of Uppsala, P.O. Box 535, S-751 21 Uppsala, Sweden
[48] IFIC, Valencia-CSIC, and D.F.A.M.N., U. de Valencia, Avda. Dr. Moliner 50, E-46100 Burjassot (Valencia), Spain
[49] Institut für Hochenergiephysik, Österr. Akad. d. Wissensch., Nikolsdorfergasse 18, A-1050 Vienna, Austria
[50] Inst. Nuclear Studies and University of Warsaw, Ul. Hoza 69, PL-00681 Warsaw, Poland
[51] Fachbereich Physik, University of Wuppertal, Postfach 100 127, D-42097 Wuppertal, Germany
[52] On leave of absence from IHEP Serpukhov

1 Introduction

The Standard Model of the electroweak interactions has proved to be in very good agreement with all experimental observations so far performed. In particular, studies done at the LEP collider have provided a wealth of very precise experimental results. However, not all observables have been experimentally investigated, especially in the field of spin asymmetries.

The transition probability for fermion-antifermion production

$$e^-(k_1) + e^+(k_2) \;\rightarrow\; f^-(p_1, s_1) + f^+(p_2, s_2) \tag{1}$$

in the Standard Model (or more generally in a model with chirality-conserving interactions) can be written [1], at tree level, as

$$\sum |M(s_1, s_2)|^2 = \frac{1}{4}|P(q^2)|^2(A + B_{1\mu}s_1^\mu + B_{2\mu}s_2^\mu + C_{\mu\nu}s_1^\mu s_2^\nu), \tag{2}$$

where s_i^μ $(i = 1, 2)$ are the covariant spin vectors of the final state particles, k_i^μ and p_i^μ are the covariant momentum vectors of the initial and final state particles respectively, $q = k_1 + k_2$, and

$$P(q^2) = \frac{e^2}{16 \sin^2\theta_W \cos^2\theta_W} \cdot \frac{q^2}{q^2 - M_Z^2 + iq^2\Gamma_Z/M_Z}, \tag{3}$$

where θ_W is the electroweak mixing angle, e is the charge of the electron, and M_Z and Γ_Z are the mass and the width of the Z boson.

The spin-independent term in equation (2) is

$$A = C_0(1 + \cos^2\theta^*) + 2C_1 \cos\theta^* \tag{4}$$

where θ^* is the f^- polar angle with respect to the e^- direction, and it is related to the total cross-section and to the forward-backward asymmetry.

The spin vector s_i^μ can be decomposed, as $s_i^\mu = s_i^L l_i^\mu + s_i^T t_i^\mu + s_i^N n_i^\mu$, into its longitudinal, transverse (within the collision plane) and normal (to the collision plane) components [1]. To leading order in the fermion mass m_f, the term linear in the spin in equation (2) is given by

$$B_{1\mu}s_1^\mu + B_{2\mu}s_2^\mu = -D_0(s_1^L - s_2^L)(1 + \cos^2\theta^*) - D_1(s_1^L - s_2^L)2\cos\theta^* \tag{5}$$

and is related to the longitudinal polarization asymmetry and forward-backward polarization asymmetry. Other terms related to transverse spin components are suppressed by $\frac{m_f}{M_Z}$ factors.

The term quadratic in the spin in equation (2) gives rise to the spin correlations, with:

$$C_{\mu\nu}s_1^\mu s_2^\nu = C_0h_0 + C_1h_1 + C_2h_2 + D_2h_3 \tag{6}$$

where C_0 and C_1 are the same coupling constants as in equation (4) and

$$\begin{aligned}
h_0 &= -s_1^L s_2^L(1 + \cos^2\theta^*) && (7)\\
h_1 &= -2s_1^L s_2^L \cos\theta^* && (8)\\
h_2 &= (s_1^N s_2^N - s_1^T s_2^T)\sin^2\theta^* && (9)\\
h_3 &= (s_1^N s_2^T + s_1^T s_2^N)\sin^2\theta^* && (10)
\end{aligned}$$

The first two terms are related to the longitudinal spin correlation, which is equal to unity by helicity conservation. The h_2 term gives rise to the transverse-transverse spin

correlation, which is the subject of this paper, and h_3 to the transverse-normal spin correlation. This last is a time-odd observable, and is generated in the Standard Model by absorptive parts in the electroweak amplitudes and by $\gamma - Z$ interference terms: its magnitude is predicted to be very small.

At tree level at the Z peak, the prediction for the transverse-transverse spin correlation is

$$C_{TT} \equiv \frac{C_2}{C_0} = \frac{|a_f|^2 - |v_f|^2}{|a_f|^2 + |v_f|^2} = 0.978 \tag{11}$$

for $\sin^2\theta_W = 0.2236$, where v_f and a_f are the vector and axial couplings of the fermion to the Z.

The measurement of this observable represents another important test of the Standard Model. In Z decays to light quarks, transverse spin analysers were proposed in [2,3]; a few measurements were performed [4–6], but no evidence of a non-zero analysing power was obtained. In the leptonic sector, a unique possibility is provided by the Z decay into τ pairs, since the subsequent parity violating decay of the τ acts as spin analyser.

Preliminary evidence of the spin correlation in $Z \to \tau^+\tau^-$ pairs was found in [7,8]. This paper presents a measurement of the transverse spin correlation parameter in τ decays, based on the data collected by DELPHI at the Z during 1992 to 1994.

2 Experimental method

The coordinate system used for the analysis is shown in Fig. 1, where $\vec{p_1}$ is the total momentum of the decay products of the τ^- excluding the neutrinos, and $\vec{p_2}$ that of the τ^+, in the laboratory frame.

After integrating over all variables except the azimuthal angle ψ of the e^- axis in this reference frame, the differential cross section, neglecting the transverse-normal spin correlation, becomes:

$$\frac{d\sigma}{d\psi} \propto 1 + \alpha_1\alpha_2 K C_{TT} \cos 2\psi \tag{12}$$

where K is a factor depending on the decay mode and the kinematics, while the α_i are the analysing powers of the two τ decays and are equal [9] to -1 for the $\tau \to \pi\nu$ channel, -0.67 for $\tau \to \rho\nu$, between -10^{-3} and -0.15 for $\tau \to a_1\nu$ depending on the a_1 mass, and $+0.2$ for the leptonic channels.

The transverse spin correlation therefore gives rise to an asymmetry in the acoplanarity (ψ) distribution of the decay products of the two taus in the Z decay, namely a $\cos 2\psi$ dependence of the cross section. Since the magnitude of the effect depends on the product of the two analysing powers, $\alpha_1\alpha_2$, it is clear that the largest effect is expected in the case where both taus decay to a pion (kaon) or to a rho (K^*), and that an effect of opposite sign is expected when one of the taus decays to a lepton.

To study the event selection and to measure the transverse spin correlation parameter, two different $\tau^+\tau^-$ event generators were used: KORALZ [10], which only includes effects due to longitudinal spin, and KORALB [11], which also has effects due to transverse spin. KORALB is a tree level generator, while KORALZ includes higher order radiative corrections based on pragmatic $\mathcal{O}(\alpha)$ exponentiated QED corrections. The events generated with KORALZ were processed through the DELPHI detector full simulation program DELSIM [12] and were used to study event selection. A fast simulation program was also developed, with parametrisations of detector effects obtained from events with full

detector simulation. The events generated with KORALB were processed through this fast simulation.

The following generators were used to study the backgrounds: DYMU3 [13] for $e^+e^- \to \mu^+\mu^-$ events, BABAMC [14] for $e^+e^- \to e^+e^-$ events, JETSET 7.4 [15] for $e^+e^- \to q\bar{q}$ events, the Berends-Daverveldt-Kleiss [16] generator for $e^+e^- \to e^+e^-e^+e^-$ events, and the generator described in [17] for $e^+e^- \to e^+e^-\mu^+\mu^-$ and $e^+e^- \to e^+e^-\tau^+\tau^-$ events. In all cases the events were processed through the full detector simulation.

The detector response was also studied using test samples of data for which the particle identity was known, such as $e^+e^- \to e^+e^-$ events and $e^+e^- \to \mu^+\mu^-$ events, and the measured resolutions were used to tune the detector simulation. For a detailed discussion of the relevant particle identification issues, see [18].

The rest of the paper is organized as follows. A brief description of the DELPHI detector is given in section 3. Event selection is described in section 4. In section 5, the value of the correlation parameter is obtained by comparing the data with the KORALB predictions. It is also shown that a value of C_{TT} compatible with zero is observed with the KORALZ Monte Carlo, which does not include the transverse spin correlation effect. In section 6, a discussion of systematic uncertainties is presented and in section 7 the final results are given.

3 The DELPHI detector

The DELPHI detector and its performance are described in detail elsewhere [19,12]. The sub-detector units particularly relevant for this analysis, which is confined to the barrel region, are summarized here. In the DELPHI reference frame the z-axis is taken along the direction of the e^- beam. The angle θ is the polar angle defined with respect to the z-axis, ϕ is the azimuthal angle around this axis, and r is the radial distance from it. The reconstruction of a charged particle trajectory in the barrel region of DELPHI resulted from a combination of the measurements in the following detectors.

- The Vertex Detector (VD) was made of three layers of 24 cm long single-sided silicon microstrip modules, at radii r of 6.3, 9.0 and 11.0 cm from the beam axis. The space point precision was about 8 μm and the two track resolution was 100 μm in $r\phi$. For the 1994 run, the inner and outer layers were replaced with double-sided silicon microstrip modules providing absolute z coordinate measurements in addition to the $r\phi$ information.
- The Inner Detector (ID) had an inner radius of 12 cm and an outer radius of 28 cm. A jet chamber measured 24 $r\phi$ coordinates and provided track reconstruction. Its two track resolution in $r\phi$ was 1 mm and its spatial precision 50 μm. It was surrounded by proportional chambers used for triggering purposes and z measurement.
- The Time Projection Chamber (TPC), extending from 30 to 122 cm in radius, was the main detector for the track reconstruction. It provided up to 16 space points for pattern recognition and ionisation information extracted from the charge deposition on up to 192 anode wires. Every 60° in ϕ there was a boundary region between read-out sectors about 1° wide, which had no instrumentation. At $\cos\theta = 0$ there was a cathode plane, which reduced the tracking efficiency in the polar angle range $|\cos\theta| < 0.035$. The TPC had a two point resolution of about 1 cm in $r\phi$ and in z, a single point precision of 250 μm in $r\phi$ and of 880 μm in z.
- The Outer Detector (OD) consisted of 5 layers of drift cells at a radius of 2 metres from the beam axis. Each layer provided a space point with 110 μm precision in $r\phi$.

These detectors were surrounded by a solenoidal magnet with a 1.2 T field parallel to the z-axis. In addition to the detectors mentioned above, the identification of the τ decay products relied on:

- The barrel electromagnetic calorimeter, a High density Projection Chamber (HPC). This detector was situated immediately outside the OD and inside the magnet coil. Seventeen radiation lengths deep for perpendicular incidence, its energy resolution was $\Delta E/E = 6.5\%$ for electrons with an energy of 45.6 GeV. It had a high granularity and provided a sampling of shower energies from nine layers in depth. It allowed a determination of the starting point of an electromagnetic shower with an accuracy of 0.003 radians in polar angle and 0.006 radians in azimuthal angle, as determined with 45 GeV electrons. The HPC had a modularity of 15° in azimuthal angle. Between modules, there was a region about 1° wide in azimuth where the resolution of electromagnetic showers was degraded and a different treatment of the data was therefore needed.
- The Hadron Calorimeter (HCAL), sensitive to hadronic showers and minimum ionising particles. It was segmented in 4 layers in depth, with a granularity of 3.75° in polar angle and 2.96° in azimuthal angle. Lying outside the magnet coil, it had a depth of 110 cm of iron.
- The barrel Muon Chambers (MUB) consisting of two layers of drift chambers, the first one situated after 90 cm of iron and the second outside the hadron calorimeter. The acceptance in polar angle of the outer layer was slightly smaller than that of the other barrel detectors and covered the range $|\cos\theta| < 0.602$. The polar angle range $0.602 < |\cos\theta|$ was covered by the forward Muon Chambers (MUF) in certain azimuthal zones.

The DELPHI trigger was highly efficient for the τ final states, due to the redundancy existing between its different components. By comparing the response of independent components, a trigger efficiency of $(99.98 \pm 0.01)\%$ was derived for $Z \to \tau^+\tau^-$ events with at least two charged particle tracks reconstructed and in the barrel region.

4 Event selection

The initial $Z \to \tau^+\tau^-$ event selection followed criteria similar to some previous DELPHI papers (see for instance [18]): however, particular care was devoted here to suppression of external backgrounds (coming from events other than $\tau^+\tau^-$), to make the distortions of the acoplanarity spectrum negligible.

Events at the Z mass peak energy were considered. In LEP1 data, the $Z \to \tau^+\tau^-$ decays appeared as two highly collimated low multiplicity jets in approximately opposite directions. The events were separated into hemispheres by a plane perpendicular to the thrust axis, where the thrust was calculated using all charged particles. The topologies containing only one charged particle per hemisphere with at least one associated hit in the vertex detector were selected. The momentum of each particle was required to be greater than $0.07 p_{beam}$ in order to be able to penetrate to the muon chambers outside the DELPHI magnet iron. The charged particle in at least one of the two hemispheres was required to lie in the polar angle region $|\cos\theta| < 0.732$.

Cosmic rays were rejected by requiring both charged particles to have a distance of closest approach to the interaction region below 4.5 cm in z and 1.5 cm in the $r\phi$ plane. Furthermore, the smaller distance of closest approach in the $r\phi$ plane had to be less than 0.2 cm. The offset in z of tracks in opposite hemispheres of the TPC is sensitive to the

time of passage of a cosmic ray with respect to the time of interaction of the beams. The particles were therefore required to have a difference in z of less than 3 cm at their closest approach to the interaction region, which corresponds to a time of passage within 220 ns of the beam crossing.

Two-photon events were removed by requiring a total visible energy in the event, E_{vis}, defined as the sum of the charged particle momenta and any unassociated energy in the HPC, greater than $0.4p_{beam}$; a total event transverse momentum greater than 0.5 GeV/c; and an isolation angle, defined as the angle between the two charged particles, greater than 170°. The isolation angle cut was also effective against residual $e^+e^- \to q\bar{q}$ background, while the visible energy cut removed possible beam-gas events.

The presence of $e^+e^- \to e^+e^-$ and $e^+e^- \to \mu^+\mu^-$ events was reduced by requiring the acollinearity ϵ between the two tracks to be larger than 0.3°, the radial momentum $P_{rad} = (|\vec{p}_1|^2 + |\vec{p}_2|^2)^{1/2}$ to be smaller than p_{beam}, and E_{vis} to be smaller than $1.6p_{beam}$. Events were also rejected if $E_{rad} = (E_1^2 + E_2^2)^{1/2}$ was larger than $0.7p_{beam}$, the variables E_1 and E_2 being the total electromagnetic energies deposited in cones of half-angle 30° about the momentum vectors of the two particles.

From this initial $Z \to \tau^+\tau^-$ sample, two different subsamples were then selected. They were the hadron-hadron sample, with both taus decaying to a π (K) or a ρ (K^*), and the hadron-lepton sample, with one of the taus decaying to an electron or a muon. Sections 4.1 and 4.2 now present the selection of hadronic and leptonic τ decays, and Sections 4.3 and 4.4 discuss the hadron-hadron and hadron-lepton event selections, including efficiencies and residual backgrounds.

4.1 Hadronic τ decays

The π (K) and ρ (K^*) τ decay channels were selected inclusively by rejecting the muon and electron decay channels and the $\pi^{\pm}\mathrm{n}\pi^0$ channels with n > 1.

Muon rejection required the particle not to be identified as a muon by the methods described in [12]. The muons which survived this selection were mainly concentrated at polar angles $\theta < 52°$ and $\theta > 128°$, where the absence of the MUB external layer leads to a reduced identification efficiency. This background was suppressed using the fact that most muons behave as minimum-ionising particles in both calorimeters. Tracks were discarded when the associated HPC energy was less than 0.3 GeV, the number of neutral electromagnetic showers in the hemisphere was zero, and the average hadronic energy per hit layer [18],

$$E_{hlay} = E_{HCAL}/N_{Hlayers}, \tag{13}$$

was such that $0 < E_{hlay} < 3$ GeV, where E_{HCAL} is the total energy associated to the charged particle in the HCAL and $N_{Hlayers}$ is the number of layers in the HCAL with deposited energy.

Electron rejection required the particle not to be identified as an electron by the method described in [20]. Moreover, when the dE/dx information was available, its pull with respect to the pion hypothesis

$$\Pi_{dE/dx}(\pi) = \frac{(dE/dx)_{meas} - (dE/dx)_{exp}(\pi)}{\sigma(dE/dx)}, \tag{14}$$

was required to be less than 2.5. In the above expression, $(dE/dx)_{meas}$ is the measured value, $(dE/dx)_{exp}(\pi)$ is the expectation value for a charged pion (dependent on its momentum), and $\sigma(dE/dx)$ is the resolution. Further rejection used the fact that most

electrons do not penetrate beyond the first layer of the HCAL: when no energy was deposited beyond the first layer, the ratio E/p of the associated energy in the HPC to the measured momentum was required to be less than 0.5, or less than 0.3 if the particle crossed the HPC through an inefficient ϕ region. Events with tracks pointing towards HPC modules known to be inefficient or dead were rejected.

To suppress background from $\pi^{\pm}\mathrm{n}\pi^0$ decay channels with $\mathrm{n} > 1$, the hemisphere was required to have two neutral showers or less, and if there were two, their invariant mass was required to be less than 0.2 GeV to be consistent with the π^0 mass hypothesis.

In order to avoid an inefficient region for various sub-detectors, each charged particle was required to be at least 1.5° away from $\theta = 90°$ when the number of neutral showers in the hemisphere was zero.

4.2 Leptonic τ decays

The leptonic τ decays were selected by requiring the charged particle to be identified either as a muon by the methods described in [12] or as an electron by the method described in [20].

4.3 Hadron-hadron topology

The hadron-hadron event topology was selected by requiring both particles to be identified as hadrons by the criteria of section 4.1 (at least one of them was required to have a dE/dx measurement).

To reduce the remaining background, mainly coming from regions of reduced HPC and MUB efficiency, some further global selection cuts were then applied.

To suppress $e^+e^- \to \mu^+\mu^-$ background, which was mainly concentrated outside the region $55° < \theta < 125°$, P_{rad} was required to be less than $0.9p_{beam}$ if both particles had an associated energy smaller than 0.5 GeV and the number of neutral showers in the event was less than 3.

To suppress $e^+e^- \to e^+e^-$ background, P_{rad} was required to be less than $0.8p_{beam}$ and E_{vis} less than $1.4p_{beam}$ when either the deposited energy in the HCAL was zero or both tracks deposited more than 95% of their energy in the first layer.

The selected sample contained 4633 events. Its composition, as obtained from the KORALZ Monte Carlo, is given in Table 1. The selection efficiency was about 20% in the full solid angle, with an internal background (i.e. coming from other τ decays) of about 30%. The external background was estimated from the simulation to be less than 0.2%.

4.4 Hadron-lepton topology

The hadron-lepton event topology was selected by requiring one particle to be identified as a hadron and the other as a lepton by the criteria of sections 4.1 and 4.2 respectively.

For this topology, the rejection of the e^+e^- and $\mu^+\mu^-$ backgrounds is more difficult since the particle identification serves this purpose in one hemisphere only.

To suppress the $e^+e^- \to \mu^+\mu^-$ background, the event was rejected if the number of neutral showers in the event was zero and the identified hadron had both an associated HPC energy smaller than 0.5 GeV and $0 < E_{hlay} < 2.5$ GeV.

To suppress the $e^+e^- \to e^+e^-$ background, P_{rad} was required to be less than $0.8p_{beam}$ and E_{vis} less than $1.4p_{beam}$. If at least one of the two tracks pointed towards a dead

region of the HPC and either the deposited energy in the HCAL was zero or more than 95% of the energy was deposited in the first layer, P_{rad} was required to less than $0.7p_{beam}$.

Further requirements were then imposed on the particle identified as a hadron. A dE/dx measurement was required. If the track pointed to a dead ϕ region of the HPC, the event was rejected. The E/p was required to be less than 0.4 if the track pointed to the inefficient region around $\theta = 90°$ and the hemisphere contained more than one neutral. If the track pointed to an active region of the HPC, the E/p cut was loosened to 0.8.

The selected sample contained 4436 events. Its composition, as obtained from the KORALZ Monte Carlo, is given in Table 1. The selection efficiency was about 11% in the full solid angle, with an internal background of about 17%. The external background was estimated from the simulation to be less than 0.2%.

5 Measurement of the transverse spin correlation

The correlation parameter C_{TT} was measured as follows. The acoplanarity distribution of the selected events was fitted with the function, based on formula (12),

$$f(\psi') = A \cdot (1 + B \cdot \cos 2\psi') \tag{15}$$

with A and B taken as free parameters, where ψ, $0° < \psi < 360°$, was replaced by ψ', $0° < \psi' < 90°$, on the basis of the symmetry of the cosine function. Then the relation between the measured B value and the corresponding C_{TT} parameter was obtained from the same fit applied to events generated with the KORALB Monte Carlo for six different values of C_{TT} ranging from 0 to 1.

The KORALB events were generated in the different topologies according to the signal and background fractions obtained from the event selection with full detector simulation. The events in the a_1 decay channel were generated with a flat acoplanarity distribution. Detector effects were parametrised using values of resolutions taken from events with full detector simulation. $\tau^+\tau^-$ selection cuts similar to those applied to the data were used.

Following the expectation of ref. [21], suggesting that τ decay particles having small momentum in the laboratory frame are less sensitive to the transverse spin effect, the events belonging to the hadron-hadron and hadron-lepton topologies were each further split into two classes according to the values of the decay particle momenta: events having both decay particle momenta above $0.3p_{beam}$ (class II) and all the others (class I). This gave a total of four event categories, numbered 1 to 4 in Table 2. The event composition, as presented in Table 1, was the same in classes I and II within errors.

The mean sensitivity per event of the C_{TT} measurement, defined as $S \equiv 1/(\Delta C_{TT}\sqrt{N})$, where N is the number of selected events and ΔC_{TT} is the error of the measurement, was obtained from event samples generated with KORALB, assuming B to be proportional to C_{TT}. From Table 2 it is seen that higher sensitivities are expected for events belonging to class II than for those belonging to class I.

The acoplanarity distributions of data events and KORALZ events with full detector simulation belonging to class II are shown for the hadron-hadron selection in Fig. 2 and for the hadron-lepton selection in Fig. 3, together with curves showing the results of the fits to formula (15).

The dependence of the fitted values of the B_i $(i = 1, 4)$ parameters on the generated C_{TT} values for the event categories 2 and 4 (hadron-hadron and hadron-lepton selections with both tracks in the high momentum range), as obtained from the KORALB simulation, is shown in Fig. 4, together with a straight line fit. Similar fits were also performed

for the other two regions. The fitted offset values were found to be statistically compatible with zero and the distribution of χ^2 indicated good consistency with the straight line hypothesis. From formula (11) it is seen that the maximum value for C_{TT} is 1 and that the Standard Model prediction is very close to this value. To take into account statistical fluctuations in the measured B_i values correctly, the fitted line was extended outside the range $C_{TT} = (0, 1)$. The correlation parameter was then extracted by intersecting the fitted lines with the measured B_i values.

The number of selected events, the results of the fits for the different categories and the combined values are presented in Table 2, both for events generated with KORALZ and processed through the full detector simulation and for the data.

The data yielded $C_{TT} = 0.87 \pm 0.20$ $(stat.)$, compatible within one standard deviation with the Standard Model prediction and incompatible with zero by more than four standard deviations.

As a cross-check, the same fits were applied to the KORALZ events with full detector simulation. After subtraction of a small bias induced by radiative effects and obtained from a very high statistics sample of events processed through the fast simulation, the KORALZ events yielded $C_{TT} = 0.08 \pm 0.10$ $(stat.)$, compatible with zero within one standard deviation.

6 Systematic uncertainties

Various sources of systematic uncertainties which might affect either the KORALB predictions, the measurement on the data, or both, were investigated.

The dependence of the measured correlation parameter on the exact values of the selection cuts was investigated by varying them around their mean values in the same way in the data and in the simulation; variations in the C_{TT} value due to the changes in the number of events were subtracted out. Correlations due to increased background contributions when relaxing some of the cuts were also taken into account. No other significant correlations were found.

A possible dependence of the selection efficiency on ψ' was also investigated. The very small correction needed was applied both to the data and to a very high statistics sample of simulated events generated with KORALB with $C_{TT} = 0$. It was found to have no significant effect either on the mean C_{TT} value or on its error.

The presence of external backgrounds in the final selection was estimated using fully simulated events with the detector response carefully tuned to reproduce the data behaviour. However, possible residual discrepancies between the data and the simulation, might have led to a wrong estimate of the background. Since this was found to be a small effect, it was treated as a systematic uncertainty on the final result. The main contribution came from uncertainties in the Bhabha background rejection, due to both imperfections in the simulation of the HPC response and to missing higher orders in the Monte Carlo generator used [14].

Contributions to the error from missing radiative corrections were also considered, taking into account the estimation of [21], and from the neglected a_1 contribution to the transverse spin correlation in the KORALB Monte Carlo.

The contribution to the systematic error coming from finite Monte Carlo statistics in the KORALB generation was estimated taking the errors (at one standard deviation) of the linear fit and determining the corresponding new values for C_{TT}.

The τ branching ratios and the value of the electroweak mixing angle were varied in the KORALB Monte Carlo to account for the uncertainties in the present world average

values [22]; the variations in the final result were negligible compared to the other sources of systematic uncertainties.

Uncertainties in the efficiency corrections obtained with the KORALB Monte Carlo were estimated to give a negligible contribution to the systematic error. It was also verified that the correlations among the selection efficiencies as a function of the acoplanarity ψ', the τ^- polar angle θ^* and the acollinearity ϵ, which could spoil the validity of equation (12) after selection cuts, were very small and could be safely neglected.

The relevant contributions to the systematic error are listed in Table 3: the total systematic error was obtained by adding the various contributions in quadrature.

7 Combined Result and Discussion

The combined value of C_{TT} from all the data samples was:

$$C_{TT} = 0.87 \ \pm \ 0.20 \ (stat.) \ ^{+\ 0.10}_{-\ 0.12} \ (syst.) \tag{16}$$

in good agreement with the Standard Model prediction.

The presence of a contribution to the acoplanarity distribution in addition to that expected from the Standard Model was tested by performing a fit with the function

$$f(\psi) = A \cdot (1 + B \cos 2\psi + D \sin 2\psi) \tag{17}$$

with A, B and D taken as free parameters. Indeed, a $\sin 2\psi$ dependence is expected from the transverse-normal spin correlation, which is predicted to be very small in the Standard Model but could receive contributions from CP-violating amplitudes.

The B_i values obtained from a fit of equation (17) to the four event classes in the data were compatible with those obtained from the two parameter fit. The D_i values for the four data categories are shown in Table 2, together with their fit to a single value. The value obtained is compatible with zero and thus in agreement with the Standard Model prediction.

In conclusion, the correlation between the transverse spin components of $\tau^+\tau^-$ pairs has been measured from a study of the acoplanarity distribution between the τ^+ and τ^- decay products with the data collected during the years 1992 to 1994 by the DELPHI detector at LEP. The value obtained for the correlation parameter is in agreement with the predictions of the Standard Model.

8 Acknowledgements

We would like to thank Z. Was for a useful discussion, the LEP technical staff for the excellent performance of the machine, and our funding authorities for their continued support.

References

[1] J. Bernabeu, N. Rius and A. Pich, Phys. Lett. **B257** (1991) 219.
[2] X. Artru and J. Collins, Z. Phys. **C69** (1996) 277.
[3] A.V. Efremov, L. Mankiewics and N.A. Tornquist, Phys. Lett. **B284** (1992) 394.
[4] W. Bonivento, A. Kotsinian and C. Matteuzzi, DELPHI Note 95-54 PHYS 491.
[5] DELPHI Collaboration, W. Bonivento et al., Contribution eps0549 to the EPS-HEP 95 Conference, Brussels, July 1995, DELPHI 95-81 PHYS 516.
[6] ALEPH Collaboration, D. Buskulic et al., Phys. Lett. **B374** (1996) 319.
[7] DELPHI Collaboration, W. Bonivento et al., Contribution eps0765 to the EPS-HEP 95 Conference, Brussels, July 1995, DELPHI 95-111 PHYS 546.
[8] ALEPH Collaboration, Contribution pa07-075 to the ICHEP-96 Conference, Warsaw, July 1996.
[9] M. Davier et al., Phys. Lett. **B306** (1993) 411.
[10] S. Jadach and Z. Was, Comp. Phys. Comm. **36** (1985) 191;
S. Jadach, B.F.L. Ward and Z. Was, Comp. Phys. Comm. **66** (1991) 276.
[11] S. Jadach et al, Comp. Phys. Comm. **85** (1995) 453.
[12] DELPHI Collaboration, P. Abreu et al., Nucl. Instr. and Meth. **A378** (1996) 179.
[13] J. E. Campagne and R. Zitoun, Z. Phys. **C43** (1989) 469.
[14] F. A. Berends, W. Hollik and R. Kleiss, Nucl. Phys. **B304** (1988) 712.
[15] T. Sjöstrand, Comp. Phys. Comm. **27** (1982) 243, ibid. **28** (1983) 229;
T. Sjöstrand and M. Bengtsson, Comp. Phys. Comm. **43** (1987) 367;
T. Sjöstrand, "PYTHIA 5.6 JETSET 7.3 Physics and manual", report CERN-TH 6488/92 (1992).
[16] F.A. Berends, P.H. Daverveldt, R. Kleiss, Phys. Lett. **B148** (1984) 489;
Comp. Phys. Comm. **40** (1986) 271.
[17] T. Todorov, "Détermination des paramètres du modèle standard et tests de sa validité dans les désintegrations hadroniques du Z ", Doctoral thesis, CRN Strasbourg, report CRN/HE 94-21, 1994.
[18] DELPHI Collaboration, P. Abreu et al., Zeit. Phys. **C67** (1995) 183.
[19] DELPHI Collaboration, P. Abreu et al., Nucl. Instr. and Meth. **A303** (1991) 233.
[20] DELPHI Collaboration, P. Abreu et al., Z. Phys. **C66** (1995) 323.
[21] F. Sanchez and Z. Was, Phys. Lett. **B351** (1995) 562.
[22] R.M. Barnett et al., Phys. Rev. **D54** (1996) 1.

	ℓ-ℓ (gen.)	h-ℓ (gen.)	h-h (gen.)	*others* (gen.)
h-h (sel.)	0.2 ± 0.1	6.0 ± 0.2	69.5 ± 0.4	24.3 ± 0.3
h-ℓ (sel.)	1.5 ± 0.1	83.2 ± 0.3	1.7 ± 0.3	13.5 ± 0.3

Table 1: Sample composition (%) for the events selected (sel.) after all the cuts in the hadron-lepton topology (h-ℓ) and in the hadron-hadron topology (h-h), derived from a study of events generated (gen.) with the KORALZ Monte Carlo with full detector simulation; ℓ stands for electron and muon decays, h for pion, rho, kaon and K^* decays, and *others* for events containing at least one τ decaying to $\pi^{\pm}\mathrm{n}\pi^0$ with n > 1. The errors are statistical only.

	h-h (1)	h-h (2)	h-ℓ (3)	h-ℓ (4)	combined	$\frac{\chi^2}{d.o.f.}$
	Class I	Class II	Class I	Class II		
KORALB - fast simulation						
S	0.04	0.09	0.02	0.07		
KORALZ - full detector simulation						
B_i	0.017 ± 0.013	-0.023 ± 0.020	0.009 ± 0.013	-0.027 ± 0.022		
N	12110	5033	12800	3902	33845	
$\frac{\chi^2}{d.o.f.}$	10/12	12/12	6/12	6/12		
C_{TT}	0.38 ± 0.22	-0.03 ± 0.13	-0.23 ± 0.38	0.22 ± 0.26	0.08 ± 0.10	4/3
data						
B_i	0.035 ± 0.024	0.119 ± 0.038	0.009 ± 0.025	-0.118 ± 0.043		
N	3329	1304	3378	1058	9069	
$\frac{\chi^2}{d.o.f.}$	21/12	5/12	16/12	7/12		
C_{TT}	0.69 ± 0.41	0.95 ± 0.27	-0.22 ± 0.73	1.37 ± 0.50	0.87 ± 0.20	4/3
D_i	-0.018 ± 0.024	0.053 ± 0.039	0.015 ± 0.023	0.041 ± 0.043	0.011 ± 0.015	3/3
$\frac{\chi^2}{d.o.f.}$	24/11	4/11	11/11	10/11		

Table 2: Measurement of C_{TT} in the four event categories ($i = 1$ to 4). In the events in Class II, both momenta are above $0.3p_{beam}$; in Class I, at least one momentum is lower than this. From top to bottom: mean sensitivity per event S (see text) obtained from the KORALB fast simulation; fitted B_i ($i = 1, 4$) values with the two parameter fit described in the text, number of selected events, $\chi^2/d.o.f.$, and measured C_{TT} values in KORALZ events with full detector simulation; then the same in data, followed by the fitted D_i values from the three parameter fits to the data described in Section 7, and their $\chi^2/d.o.f.$ values.

variation of cuts	
momentum cut separating classes I and II	$^{+\ 0.01}_{-\ 0.04}$
momentum acceptance of tracks	$^{+\ 0.06}_{-\ 0.02}$
total transverse momentum	± 0.03
E_{vis}	$^{+\ 0.01}_{-\ 0.05}$
E_{rad}	$^{+\ 0.05}_{-\ 0.01}$
P_{rad}	$^{+\ 0.01}_{-\ 0.03}$
E/p	$^{+\ 0.01}_{-\ 0.03}$
HCAL energy	± 0.02
other contributions	
external backgrounds	± 0.03
missing higher orders in KORALB	$^{+\ 0.00}_{-\ 0.05}$
missing a_1 contribution to C_{TT} in KORALB	$^{+\ 0.00}_{-\ 0.03}$
Monte Carlo statistics	$^{+\ 0.03}_{-\ 0.04}$
total	$^{+\ 0.10}_{-\ 0.12}$

Table 3: Contributions to the systematic error on C_{TT}.

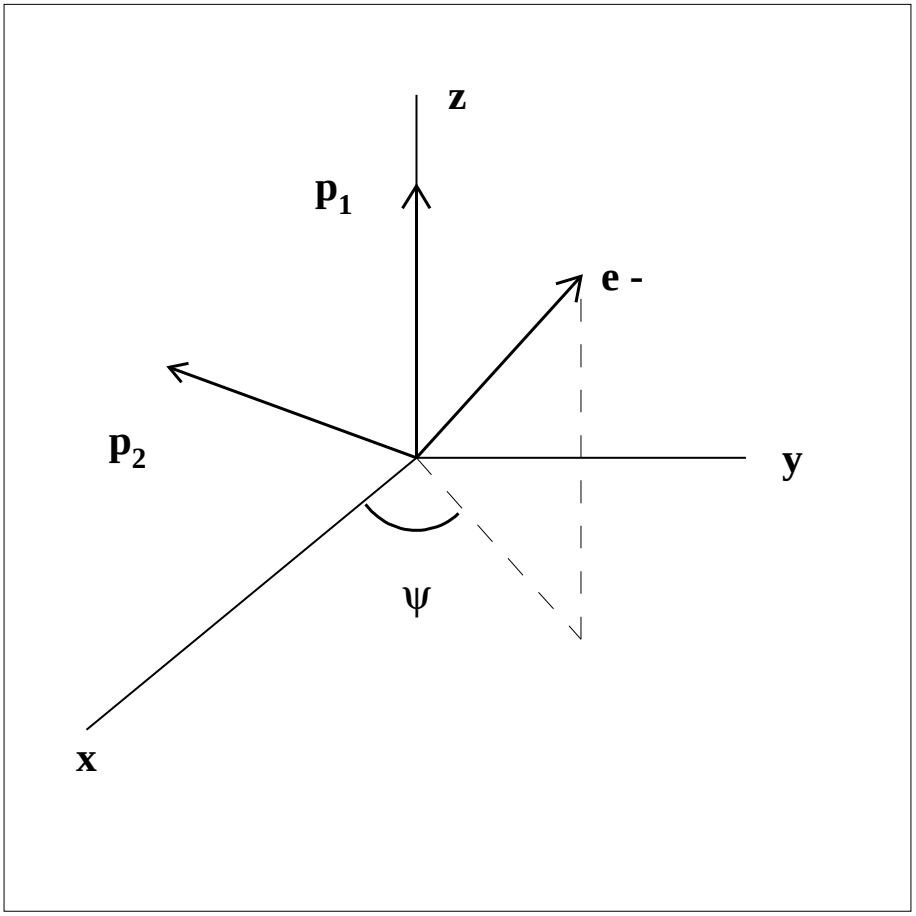

Figure 1: Coordinate system in the laboratory frame used to define the acoplanarity angle ψ in the process $e^+e^- \to \tau^+\tau^-$: $\vec{p_1}$ and $\vec{p_2}$ are the total momenta of the decay products of the τ^- and τ^+ respectively, excluding the neutrinos, $\vec{p_1}$ defines the z axis, $\vec{p_2}$ lies in the $x-z$ plane, ψ is the azimuthal angle about the z axis of the incident beam e^- in this reference frame.

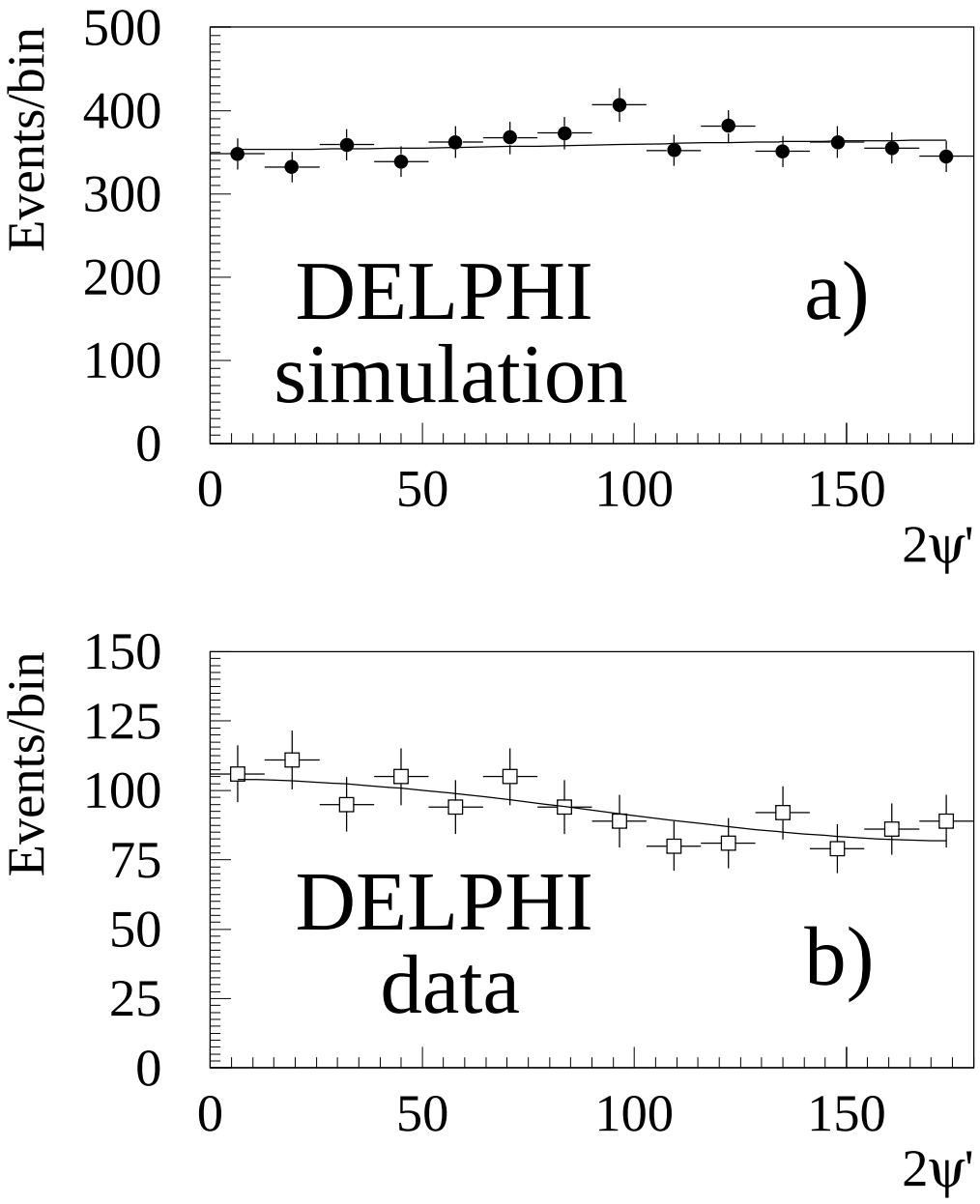

Figure 2: Acoplanarity distribution (see text) for selected events belonging to class II (both track momenta above $0.3p_{beam}$) in the **hadron-hadron** topology **(a)** for events simulated with KORALZ (without the transverse spin correlation effect) and full detector simulation, and **(b)** for the data. The *curves* are the results of the 2-parameter fit described in the text.

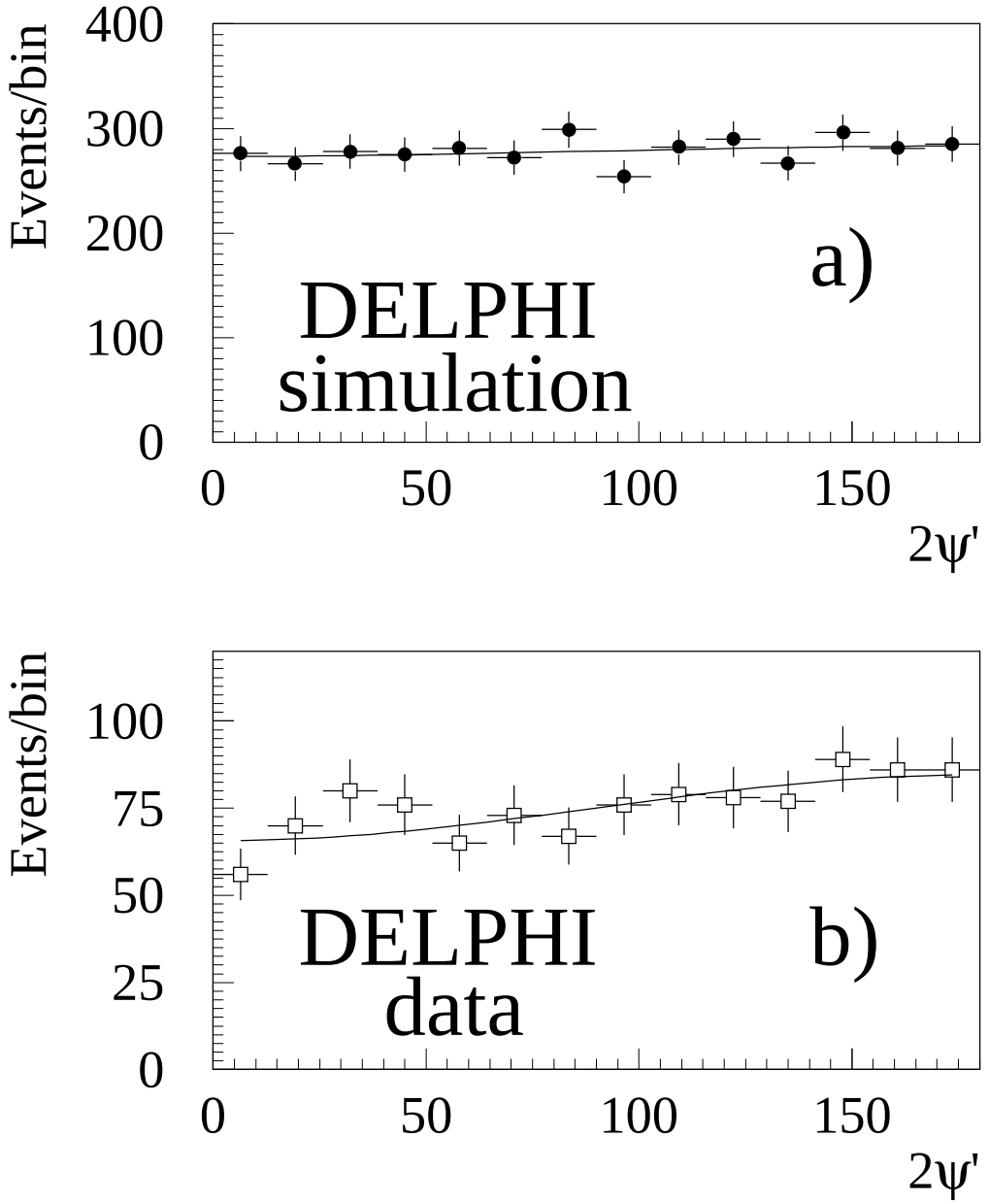

Figure 3: Acoplanarity distribution (see text) for selected events belonging to class II in the **hadron-lepton** topology **(a)** for events simulated with KORALZ (without the transverse spin correlation effect) and full detector simulation, and **(b)** for the data. The *curves* are the results of the 2-parameter fit described in the text.

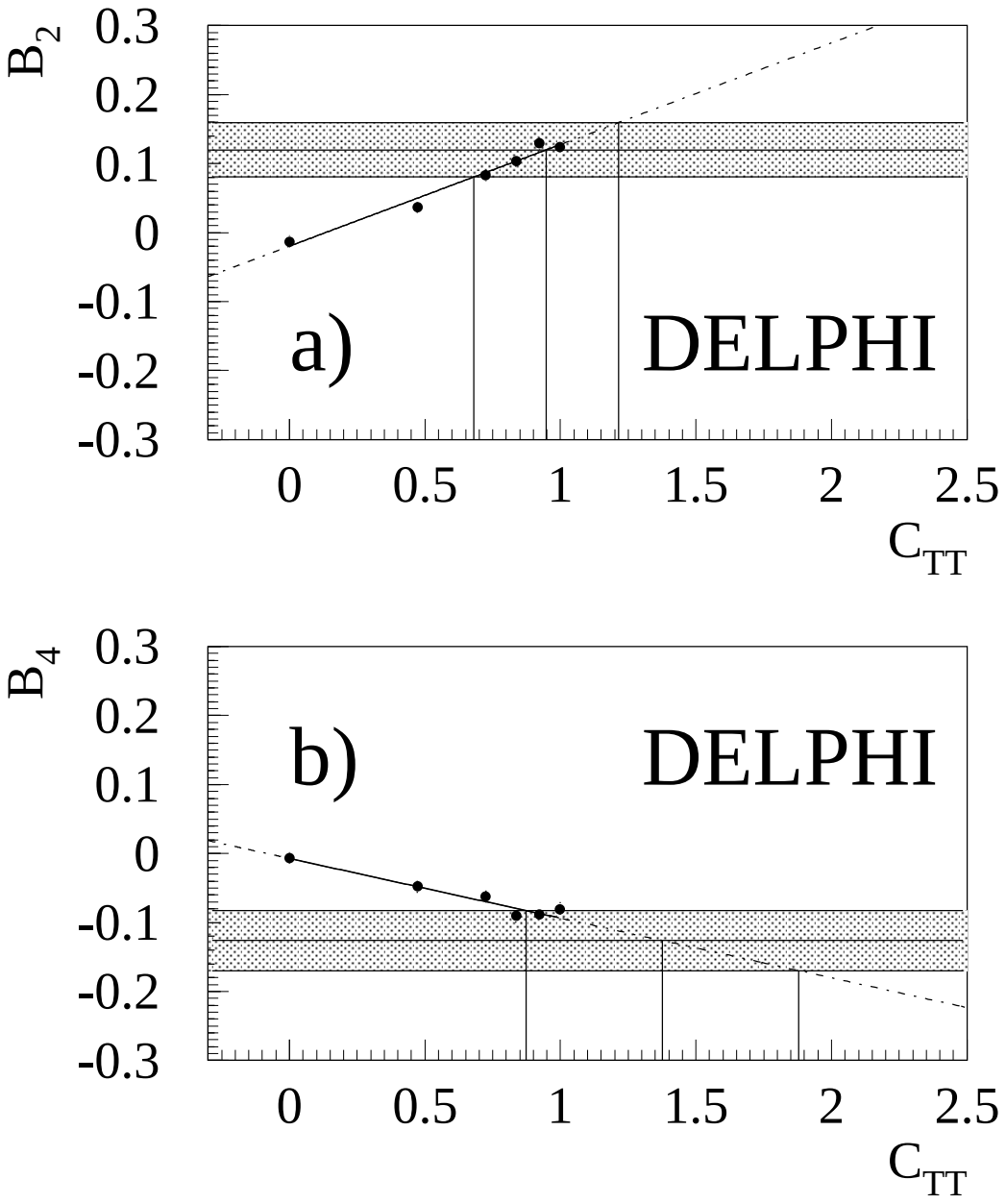

Figure 4: The full circles show the fitted values of **(a)** B_2 and **(b)** B_4 versus the input correlation parameter C_{TT} for events generated with the KORALB Monte Carlo. B_2 was obtained with a fit to data belonging to class II in the hadron-hadron topology, while B_4 with a fit to data belonging to class II in the hadron-lepton topology. Straight line fits are superimposed. The shaded bands correspond to the ± 1 standard deviation variations of the values measured on the data.